10-1-2011

A Search for MRI diffusion coefficient standards

Hongmei Yuan

A Search for MRI Diffusion Coefficient Standards

Hongmei Yuan

M.S. Physical Chemistry, Wuhan University, Wuhan, P.R.China, 2004
B.S. Chemical Education, Xinyang Normal University, Xinyang, P.R.China, 2001

A dissertation submitted in partial fulfillment of the
requirements for the degree of Master of Science in the
Department of Chemistry,
College of Science
Rochester Institute of Technology

October 2011

Signature of the Author _____

Accepted by _____
Director, M.S. Degree Program Date

DEPARTMENT OF CHEMISTRY
COLLEGE OF SCIENCE
ROCHESTER INSTITUTE OF TECHNOLOGY
ROCHESTER, NEW YORK

CERTIFICATE OF APPROVAL

M.S. DEGREE DISSERTATION

The M.S. Degree Dissertation of Hongmei Yuan has
been examined and approved by the dissertation
committee as satisfactory for the dissertation required for
the M.S. degree in Chemistry.

_____
Dr. Joseph Hornak, *Dissertation Advisor*

_____
Dr. Christopher Collison

_____
Dr. Lea Michel

_____
Dr. Thomas Smith

_____
Date

Abstract

Diffusion coefficients (D) can be readily measured by nuclear magnetic resonance (NMR) spectroscopy and magnetic resonance imaging (MRI) instruments. Operators of these instruments often utilize standards with known diffusion coefficients to rapidly and conveniently test the performance of the NMR or MRI system to measure diffusion. A variety of these standards have been proposed in the scientific literature. This thesis describes a diffusion standard based on water constrained by container geometry, specifically water between tightly packed, parallel glass fiber filaments. The restricted diffusion of water in this environment gives a diffusion coefficient which is selectable by the choice of data acquisition parameters. Thus, one standard can be used to achieve multiple diffusion coefficients and replaces the need for multiple diffusion standards.

Educational training was performed on a 300 MHz NMR spectrometer located at Rochester Institute of Technology (RIT). As a part of this training, pulsed magnetic field gradient strengths were calibrated and diffusion coefficients (D) measured for a series of silicone oils of different viscosities.

Diffusion coefficient values for a small diameter test phantom were measured on a 600 MHz NMR spectrometer with stimulated echo pulse sequence at 25 ℃. A predictable behavior between the apparent diffusion coefficient and gradient separation (Δ) value in the sequence was observed. Diffusion coefficient values were measured for a larger diameter phantom using a 1.5 T imager at 20 ℃ using echo-planar imaging sequence and confirmed to follow the same D vs. Δ behavior. Based on these observations, a hydrated fiber bundle can make a diffusion phantom with only water yielding the NMR signal.

ACKNOWLEDGEMENT

My deepest thanks to Dr. Joseph Hornak, my research advisor. This thesis would not have been possible without Dr. Hornak's great assistance and encouragement. Thanks also to Dr. Hornak's wife, Elizabeth Hornak, whose enthusiasm and kindness makes me feel like a part of an American family. Thanks to my other thesis committee members, Dr. Thomas Smith, Dr. Christopher Collison, Dr. Andreas Langner, and Dr. Lea Michel, for their assistance and encouragement during my studies at Rochester Institute of Technology. I am especially thankful to Dr. Paul Rosenberg, Brenda Mastrangelo, and Autumn Madden for their care and attention, as well to the RIT Chemistry Department for supporting me.

I also wish to thank Dr. Scott Kennedy at the University of Rochester Biophysics & Biochemistry, Dr. Edmund Kwok from the Imaging Science Department at the University of Rochester Medical Center, Dr. Paul Keifer at Varian Inc., and Dr. Amy Freund at Bruker Biospin Inc., who have supported instruments and measurements in this work.

Special thanks should be given to my ESL teachers, Lisa Hoffmaster and Linda Gamlen, to my student colleagues, Can Wang, Yuqiong Joan Wang, Yujie Qiu and her husband, Wei Yao, Jennifer Swartzenberg, and Luticha A. Doucette, who helped me in many ways in America. Finally, words alone cannot express the thanks I owe to my family members in China and Shunxu Ge, my husband for their encouragement and assistance.

Table of Contents

1.0 Introduction

In the last three decades, magnetic resonance imaging (MRI) has established itself as the most diagnostically useful imaging modality in the medical imaging field. It is in part because of the ability of MRI to distinguish between soft tissues in the body. The last decade has seen the emergence of a new kind of MRI, quantitative MRI. Quantitative MRI uses MRI to measure some specific property, such as the diffusion coefficient, and relate it specifically to a disease state.

Some studies have related the diffusion coefficient of water in tissues to a disease state such as ischemia [1-4], epilepsy [5-7], tumors [8-10], and strokes [11-13]. Magnetic resonance imaging is capable of producing several forms of images yielding diffusion information. These include diffusion weighted, diffusion, and diffusion tensor images. Diffusion weighted images are magnetic resonance images where contrast is related to the diffusion coefficient. Diffusion imaging produces images of the diffusion coefficient. Diffusion tensor imaging (DTI) produces images of the diffusion tensor of water in each location in the image. The technique has been especially useful in mapping the tracks of nerve fibers in the brain, and therefore determining interconnectivity in the brain.

Quantitative magnetic resonance imaging studies of diffusion require a standard, or phantom, to calibrate the imaging system. A phantom is an anthropogenic object used to test the performance of the imaging system. The term phantom is more commonly used by the MRI community. Several diffusion phantoms have been proposed in the literature. These include liquids with an isotropic D value [14-17], plants [18-20], biological [21-23], capillary [23-25], and fiber [26-27] phantoms.

Phantoms utilizing isotropic liquid consists of a set of hydrocarbon liquids with self diffusion coefficients (D) between that of water and approximately $0.5x10^{-9}$ m^2/s. [17] Shipping constraints make commercializing phantoms containing flammable hydrocarbons more costly. Plants and biological based phantoms are difficult to keep for long periods of time as they degrade and the diffusion coefficient changes. Capillary phantoms have a low signal, because a large amount of the phantom volume is the capillary tube compared to the smaller amount of signal bearing liquid, which causes large susceptibility artifacts in the images.

Phantoms based on fibers overcome many of the previously mentioned shortcomings and have some notable advantages, namely the ability to calibrate and characterize DTI. Several fiber phantoms have been reported recently [28-29] for quantitative studies. Lorenz, et al. [28] reached the conclusion that the hydrophobic fiber materials polyamide and Dyneema® (an ultra-high molecular weight polyethylene [30]), showed greater anisotropy, as well as much higher alignment along the actual fiber direction than the hydrophilic fiber materials hemp, linen, and viscose rayon. Fieremans, et al. [29], introduced a fiber phantom made of ultrahigh-molecular-weight polyethylene (micro dyneema). This kind of fiber phantom was proved to be suitable for the quantitative validation of diffusion imaging because of the correspondence between the simulations and the experimental results. The result of their three-dimensional Monte Carlo simulation of random walker demonstrated that the diffusivity for the random packing geometries with a fixed diameter was similar to the diffusivity for a random packing with a variable diameter. It is assumed that in the white matter fiber in the brain,

there is intracellular and extracellular diffusion [31], but currently, fiber materials with such exact diffusion properties are not available.

This thesis proposes a diffusion phantom based on the restricted diffusion of water between tightly packed glass fibers. This form of phantom has been developed for diffusion tensor imaging [28-29, 32-35], but not as a solution to the stated problem. This phantom should yield a range of diffusion coefficients less than D_{water} as a consequence of restricted diffusion using only water as the nuclear magnetic resonance signal bearing liquid. As a consequence, shipping of the phantom should be easier.

This thesis describes a project designed to test the hypothesis that a phantom based on restricted diffusion can be used as a calibration standard for MRI. There are two parts to the test. Restricted diffusion samples will be designed, prepared and tested on a high-resolution NMR spectrometer capable of measuring diffusion coefficients. Once a standard is developed on this system, it will be scaled up in size and tested on a clinical system. I planned to use the Bruker DRX 300 MHz NMR spectrometer located in the RIT Chemistry Department for the first phase of the project. The calibration of the system was completed but, unfortunately, a series of maintenance problems with the spectrometer forced us to look elsewhere for these measurements. Therefore all tests on high resolution systems were performed on a 600 MHz system located at the University of Rochester. The calibration results were included in this thesis to explain the process, but the University of Rochester performed their own gradient calibration procedure. MRI studies on a scaled up system were performed as planned on a clinical MRI system.

2.0 Background and Theory

2.1 Diffusion

Diffusion is the random movement of molecules or particles due to the kinetic energy of the molecules and particles. This definition is broad and covers a great deal of science. To help the reader see the connection of this research to the field of diffusion, a broad overview of diffusion will be presented first, followed by a focus on aspects more specific to this research.

The introductory student of diffusion will encounter several terms that should be described first. These include self, mutual, counter, free, restricted, anisotropic, isotropic, translational, and rotational diffusion; in addition to the true and apparent diffusion coefficients. Self-diffusion is the motion of a particle when the concentration gradient is zero. This motion is what we are familiar with when we say Brownian motion. Mutual or Counter diffusion is the motion of a particle in the presence of a concentration (C) gradient. Mutual or Counter diffusion is described by Fick's laws [36] of diffusion.

Fick's first law of diffusion describes the diffusion of particles from a region of high concentration to a region of low concentration. (See Fig. 2.1.) The flux (J) in the x direction is a result of a concentration gradient ($\partial C/\partial x$). The flux goes from regions of high concentration to regions of low concentration. J is proportional to $\partial C/\partial x$ by a constant called the diffusion coefficient (D) for the diffusing particles.

$$J = -D\,(\partial C/\partial x) \tag{2.1}$$

Fick's second law of diffusion describes the change of concentration with respect to time (t).

$$(\partial C/\partial t) = D\,(\partial^2 C/\partial x^2) \tag{2.2}$$

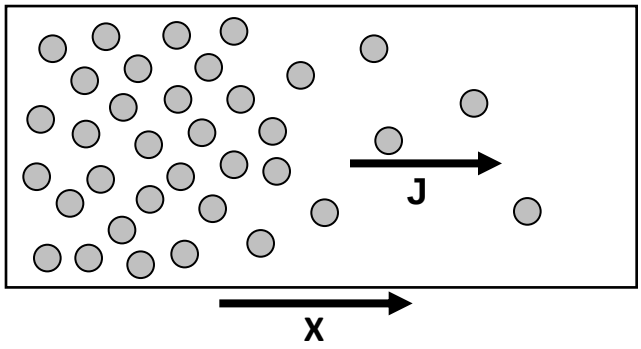

Figure 2.1 Mutual or Counter diffusion of particles in the x direction as a consequence of a concentration gradient in x.

For spherical particles of radius r, the self diffusion coefficient in absence of a concentration gradient at temperature T is directly related to the viscosity (η) of a material through the Stokes-Einstein equation [37],

$$D = \frac{k_B T}{6 \pi \eta r} \tag{2.3}$$

where k_B is the Boltzmann constant. The diffusion coefficient is temperature dependent and increases with increasing temperature. The diffusion coefficient in the international system (SI) of units has units of m^2/s. The self diffusion coefficient of water at 25 ℃ is 2.299×10^{-9} m^2/s [38].

Diffusion can be classified as restricted and unrestricted. Unrestricted diffusion is what occurs in outer space where there are no boundaries. Because most physical experiments are performed on Earth and are constrained by boundaries of one form or another, there is restricted diffusion. In practice, we can talk about both unrestricted and restricted diffusion on Earth. Unrestricted or free diffusion is the diffusion unlimited by

the size of the container, while restricted diffusion is the diffusion limited by the size of the container. Diffusion can be restricted in one, two, or three spatial dimensions.

It is possible in ordered media to have diffusion vary with direction. Examples of ordered media include nematic, smectic, cholesteric, columnar phases of liquid crystals; water bound on a surface; and mono- and bi-layers of surfactant-like molecules. It is also possible to have diffusion vary with the shape of a container. Figure 2.2 shows examples of restricted and less restricted diffusion due to the shape of the container. Diffusion of particles in a narrow cylinder with long axis along Z may experience unrestricted diffusion in Z but restricted diffusion in X and Y. The diffusion of particles within a large sphere will experience less restricted diffusion, especially on a short time scale. This introduces the need to think of the diffusion timescale. In the case of any shaped container, diffusion is unrestricted if the particles do not encounter the wall of the container during the time of a measurement. If they do encounter a wall there is restricted diffusion. The root-mean-squared distance traveled by a particle in time t is given by Eqn. 2.4, where q_i is a dimensionality constant which accounts for the dimensionality of the container [37]. The constant takes on values of 2, 4, and 6 for respectively 1, 2, and 3 dimensions.

$$\langle x \rangle^2 = q_i D t \tag{2.4}$$

It is worth mentioning at this point that the material composition of a container can have an effect on the liquid within it. For example, a polar solvent such as water in a hyrdophylic container will form a layer of bound water on the surface. This surface layer of water has very different properties than bulk or free water far from the surface. The surface water acts more like ice than free water. In a container on the order of mm or

larger in diameter, this bound layer is insignificant compared to the total volume of water. At micrometer diameter dimensions and smaller, the volume of this layer becomes significant. Therefore, water in small capillary tubes and between the fibers of a tightly packed set of fibers will exist in two forms: bulk and bound. The bound water will possess a diffusion coefficient different than bulk water. Measurements of water in these environments can yield two values: a small D value for the bound water and a larger one for the bulk water.

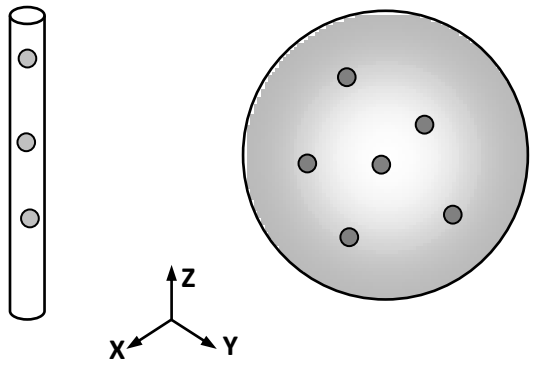

Figure 2.2 A depiction of restricted and unrestricted diffusion in a narrow cylinder and a large sphere. In the cylinder, diffusion is restricted in X and Y while unrestricted in Z. In the cylinder $D_X = D_Y \neq D_Z$, while in the sphere $D_X = D_Y = D_Z$

Diffusion, which is the same in all dimensions, is called isotropic, while anisotropic diffusion is not the same in all directions. For anisotropic diffusion, D is not the same in all directions, while for isotropic diffusion, D is independent of direction. A diffusion tensor can be used to describe anisotropic diffusion.

A tensor is an abstract object used to express a multi-dimensional concept. It can be used to represent the diffusion coefficient in three dimensions or six directions. The

following three-dimensional tensor expresses the diffusion in a narrow cylinder as depicted in Fig. 2.3.

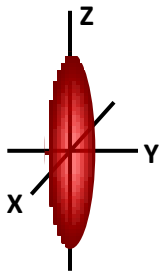

Figure 2.3 A pictorial representation of a diffusion tensor.

Thus far, the presentation of diffusion has been restricted to translational diffusion or the motion of the particles as a whole unit. Although not the subject of this thesis, it is possible to discuss rotational diffusion. Rotational diffusion is the motion of part of a molecule rotating around a bond. An example of this is the rotation of methyl hydrogens when the methyl group rotates about the carbon bond. (See Figure 2.4.)

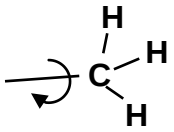

Figure 2.4 A schematic representation of rotational diffusion of the hydrogen atoms on a methyl group about a carbon bond.

Scientists often distinguish between two diffusion coefficients: the true diffusion coefficient (TDC) and apparent diffusion coefficient (ADC). The TDC is the diffusion coefficient for free diffusion, while the ADC is the measured diffusion coefficient. For restricted diffusion, the ADC is less than the TDC because the size of the container limits the diffusion distance.

2.2 Nuclear Magnetic Resonance

Electrons, protons, and neutrons possess a fundamental, quantum mechanical property of matter called spin. The spin of each of these particles can take on values of +½ and –½ [38]. The property spin can be thought of as a magnetic moment possessed by the particle. The spin of particles in close proximity can combine to give a net spin and magnetic moment of zero or some higher value. For example, a molecule or atom with two unpaired electrons in a triplet configuration will have possible spin values of +1 , 0, and –1. A nucleus with a single unpaired proton, such as hydrogen, will have values of +½ and –½, while the nucleus of sodium-23 with one unpaired proton and two unpaired neutrons can have spin values of 3/2, 1/2, -1/2, and -3/2.

When placed in a magnetic field, matter with a non-zero spin can absorb characteristic energies due to a splitting of the energy states of the spins [39-41]. Two spectroscopies focus on this absorption of energy. Electron spin resonance (ESR) spectroscopy focuses on matter with electron spin, while nuclear magnetic resonance (NMR) spectroscopy focuses on matter with nuclear spin. This thesis focuses on the use of NMR spectroscopy to measure diffusion, so the remaining theory will focus on NMR.

For a simple spin ½ nucleus, such as a hydrogen-1 nucleus, the spin has two energy levels when placed in a magnetic field (B_o). The energy difference (ΔE) between these two levels is given by

$$\Delta E = h\nu \tag{2.5}$$

where h is Planck's constant, and ν is the frequency of a photon. The value of ν can be determined using the following equation:

$$\nu = \gamma B_o \tag{2.6}$$

where γ is a proportionality constant called the gyromagnetic ratio for the nucleus. For hydrogen, $\gamma = 42.58$ MHz / T [39-41]. In the classical picture of magnetic resonance, ν is the rate at which a particle with spin precesses about the direction of the applied magnetic field.

The relative populations of the two levels (N^+ and N^-) at temperature T is given by Boltzmann statistics where k is Boltzmann's constant.

$$N^-/N^+ = e^{-\Delta E/kT} \tag{2.7}$$

The net magnetization (M) from a group of spins is proportional to ($N^+ - N^-$). It is the value of M that is probed in NMR spectroscopy. At equilibrium, the net magnetization takes on a value M_o. The NMR experiment can perturb the value of M making it other than the value M_o. Following the return of M to M_o can provide useful information about a physical system.

If the population difference of the two spin states is not at equilibrium, the distribution wants to return to equilibrium. The driving force returning the spins to equilibrium is random molecular motions at ν and 2ν which produce time varying magnetic fields (photons) which cause transitions between the energy levels and hence reestablish equilibrium. This process is called spin-lattice relaxation [39]. Spin-lattice relaxation is a first order kinetic process which is governed by a first-order time constant called the spin-lattice relaxation time (T_1).

Since particles with spin are said to precess about the direction of an applied magnetic field, it is possible to cause a sample to possess a component of magnetization

perpendicular to the direction of B_o. This transverse magnetization does not exist at equilibrium as there is no phase coherence of the precessional motion. If a transverse component of magnetization is established in a sample, it will eventually be lost due to spin exchange between nuclei and due to the spins existing in an inhomogeneous applied magnetic field. The loss of transverse magnetization is referred to a spin-spin relaxation. Spin-spin relaxation is characterized by a first order decay time constant called the spin-spin relaxation time. Magnetic resonance scientists distinguish between spin-spin relaxation processes caused by the intramolecular spin exchange (T_2) and those caused by an inhomogeneous magnetic field ($T_{2Inhomo}$). The combined spin-spin relaxation is referred to as T_2 star (T_2*) [39]

$$1/T_2^* = 1/T_2 + 1/T_{2Inhomo} \tag{2.8}$$

A spin system can be caused to have an $M \neq M_o$ and a transverse magnetization by the application of an oscillating magnetic field (B_1) (again photons) at ν_o. In magnetic resonance we adopt a Cartesian coordinate system to describe this process. In this example, B is applied along +Z and M can have an X, Y, and Z component. The system of coupled differential equations which describe the classical behavior with respect to time of magnetization from a spin system are called the Bloch equations. For simplicity, the Bloch equations [39] are often presented for a frame of reference rotating at ν_0 about Z. This rotating frame is referred to as the (X',Y',Z) frame of reference.

$$dM_{X'}/dt = 2\pi(\nu_o - \nu)\, M_{Y'} - M_{X'}/T_2 \tag{2.9}$$

$$dM_{Y'}/dt = -2\pi(\nu_o - \nu)\, M_{X'} + 2\pi\gamma B_1 M_Z - M_{Y'}/T_2 \tag{2.10}$$

$$dM_Z/dt = -2\pi\gamma B_1 M_Z - (M_Z - M_{Z_0})/T_1 \tag{2.11}$$

The Bloch equations can be solved to show the behavior of magnetization after or during any perturbation. For example, the application of a B_1 field along X' for a period of time τ will rotate M about X' by θ.

$$\theta = 2\pi \gamma B_1 \tau \tag{2.12}$$

If M is rotated from its equilibrium position along +Z to +Y' by what is called a 90^o B_1 pulse along X', M_z will return to M_o according to

$$M_Z = M_o(1-e^{-t/T_1}). \tag{2.13}$$

Transverse Y' magnetization at ν_o behaves according to

$$M_{Y'} = M_o\, e^{-t/T_2}\,, \tag{2.14}$$

while $M_{X'} = 0$ under these conditions. When $\nu \neq \nu_o$, transverse magnetization precesses about Z at frequency $(\nu-\nu_o)$ and exponentially decreases to zero.

$$M_{X'} = -\mathrm{Sin}(2\pi(\nu-\nu_o)t)\, e^{-t/T_2} \tag{2.15}$$

$$M_{Y'} = \mathrm{Cos}(2\pi(\nu-\nu_o)t)\, e^{-t/T_2} \tag{2.16}$$

2.3 Pulse Sequences

Equations (2.13) through (2.16) form the basis of a simple magnetic resonance experiment and signal. Magnetization is perturbed from equilibrium and evolves back toward equilibrium. The evolution towards equilibrium causes time varying magnetic fields in the sample which can induce a current in a coil of wire placed in a transverse place and adjacent to the sample. The signal generated by $M_{y'}$ and $M_{x'}$ is called a free induction decay (FID) [37, 39]. The FID decays exponentially with time constant T_2^* [39].

The previous example described a simple 90°-FID pulse sequence. (See Fig. 2.4.) A pulse sequence is the application of one or more B_1 pulses which generate a signal from the sample. There are numerous pulse sequences. The 90°-FID pulse sequence applies a 90° B_1 pulses which creates an FID. The FID is a time domain signal which can be Fourier transformed to produce a frequency domain representation of the frequencies in the sample.

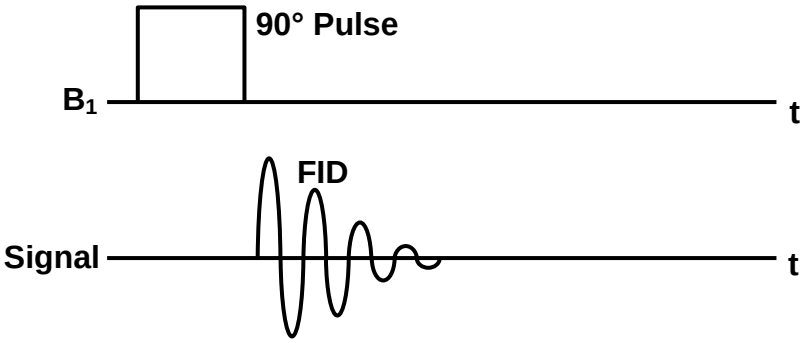

Figure 2.5 A timing diagram for a 90°-FID pulse sequence.

Another common pulse sequence is the spin-echo pulse sequence. (See Fig. 2.6.) The spin-echo sequence consists of two B_1 pulses, one 90° and one 180° pulse. The 90° pulse rotates magnetization into the XY-plane where it dephases according to T_2*. The 180° pulse refocuses the magnetization and creates a signal called an echo. The echo grows and decays exponentially according to T_2* [39, 41]. The echo amplitude (S) decays from its maximum value (S_o) when the time between the 90° pulse and the 180° pulse (T_E) is zero.

$$S = S_o \, e^{-T_E / T_2} \tag{2.17}$$

The spin-echo sequence is special because it allows the separation of spin-lattice relaxation processes from molecular interactions and spin-lattice relaxation processes from inhomogeneities in the magnetic field. The echo grows and decays according to T_2^* while the echo amplitude decays exponentially with respect to T_E with T_2.

One additional aspect of the spin-echo sequence is worth noting because of its relevance to diffusion. Assuming spins are located in an inhomogeneous magnetic field, the signal from moving spins does not completely refocus at T_E, while the magnetization from stationary spins will. This forms the basis of the pulsed magnetic field gradient diffusion measuring techniques.

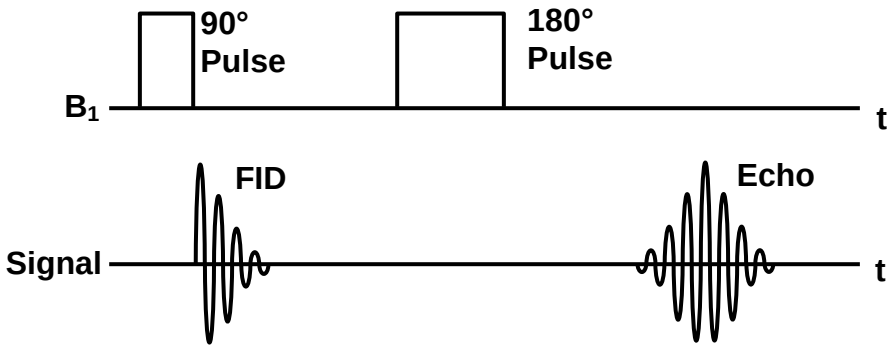

Figure 2.6. A timing diagram of the spin-echo pulse sequence

Consider the spin-echo pulse sequence of Fig. 2.7. It differs from that of Fig. 2.6 by the addition of two periods of time when a linear one dimensional gradient in the B_o magnetic field is turned on. The gradients in the B_o field are momentarily applied. The first gradient pulse causes spins at different locations in the gradient direction to precess at different rates according to their position in the gradient direction. The second gradient pulse allows reversal of any dephasing that occurred due to the first pulse when

the spins are stationary. Spins that move to a new location between the first and second gradient pulse are not refocused, and diminish the amplitude of the echo. Therefore, the echo amplitude becomes a function of the diffusion coefficient of the spins. This pulse sequence is referred to as a pulsed field gradient spin echo (PGSE) sequence [37, 39, 41].

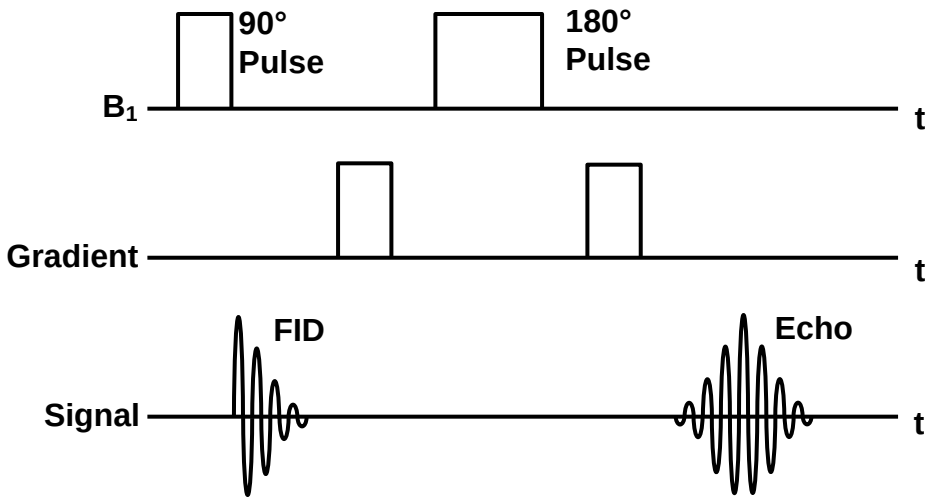

Figure 2.7. A timing diagram of the pulsed field gradient, spin-echo pulse sequence

The signal (S) in the presence of the gradient (G_{Diff}) compared to the signal in the absence of the gradient (S_o) is given by Eqn. 2.18 [41]

$$\frac{S}{S_o} = e^{-bD} \tag{2.18}$$

where

$$b = (2\pi\gamma)^2 G_{Diff}^2 \left[\delta^2 \left(\Delta - \frac{\delta}{3} \right) + \frac{\zeta^3}{30} - \frac{\delta\zeta^2}{6} \right]. \tag{2.19}$$

The gradient pulse quantities Δ, δ, and ζ refer to pulse separation, width, and risetime respectively, as defined in Fig. 2.8.

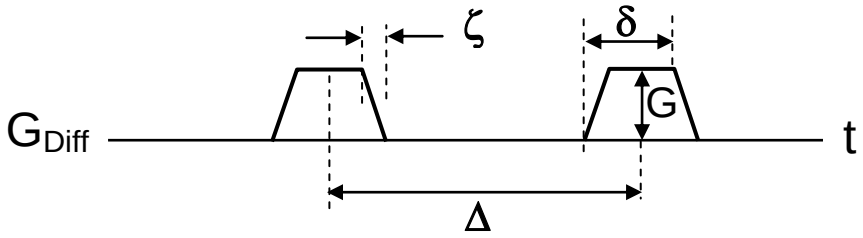

Fig. 2.8. Definition of the gradient pulse separation (Δ), width (δ), and risetime (ζ).

The diffusion gradient must be one-dimensional (1D), linear, and well characterized. D is often determined.

A detailed scientific description of the PGSE sequence can be very lengthy without analogies. The race track analogy will be used to describe the effect of the PGSE sequence on a spin system. The reader is instructed to refer to Fig. 2.9 while reading this description. Figure 2.9 presents the timing diagram and pictures of a subset of four spins in the NMR sample tube. The precessional frequency and phase of the magnetization from the set of spins is depicted as runners on a race tract. The gradients in the PGSE sequence are applied along the Z direction in this depiction such that the magnetic field at any point along Z is $(B_o + ZG_z)$. The speeds of the spins in this description are relative to the rotating frame frequency implying that spins experiencing B_o at Z=0 do not precess. For this presentation the spin-spin and spin-lattice relaxation times are assumed to be infinite.

If there is no diffusion between the application of the 90° RF pulse and the first gradient pulse, spin #1 goes around the track with the fastest speed because the gradient pulse speeds up the spin. The spin #4 goes fast in the opposite direction because of a reverse magnetic field contribution from the gradient. Spins #2 and #3 go around the

track at slower speeds in opposite directions. Each spin acquires a phase which is proportional to its position Z. The spins reverse direction after the 180 ºpulse. Because they experience the same magnetic field the gradient pulse before and after the 180 ºpulse, the spins come back to their starting position at the peak of the echo. In reality, the spins will not come back into phase completely due to spin-spin relaxation. The configuration of all spins being aligned gives a large signal.

If diffusion occurs during the pulse sequence, the movement of the spins on the racetrack looks different. (See Fig. 2.9b.) After the 90 ° RF pulse and during the first gradient pulse, the spins rotate with the same speed and the same directions as they did in Fig. 2.9a. Now we assume they can move randomly among the different tracks. Before the 180 ° RF pulse the four spins are in different tracks. There is nothing specific about the order presented in the figure, the important point is they are randomized. The 180° pulse does the same thing as in Fig. 2.9a, it flips the four spins to the other side. The gradient pulse is turned on again and spins move at specific rates around the tracks depending on their position. Because of diffusion the spins can end up on different tracks and they do not come back to the starting line in phase. We now see less signal than the case without diffusion. In reality the spins are constantly diffusion. The lost signal is related to the diffusion coefficient, the gradient strength, gradient length, and gradient pulse separation.

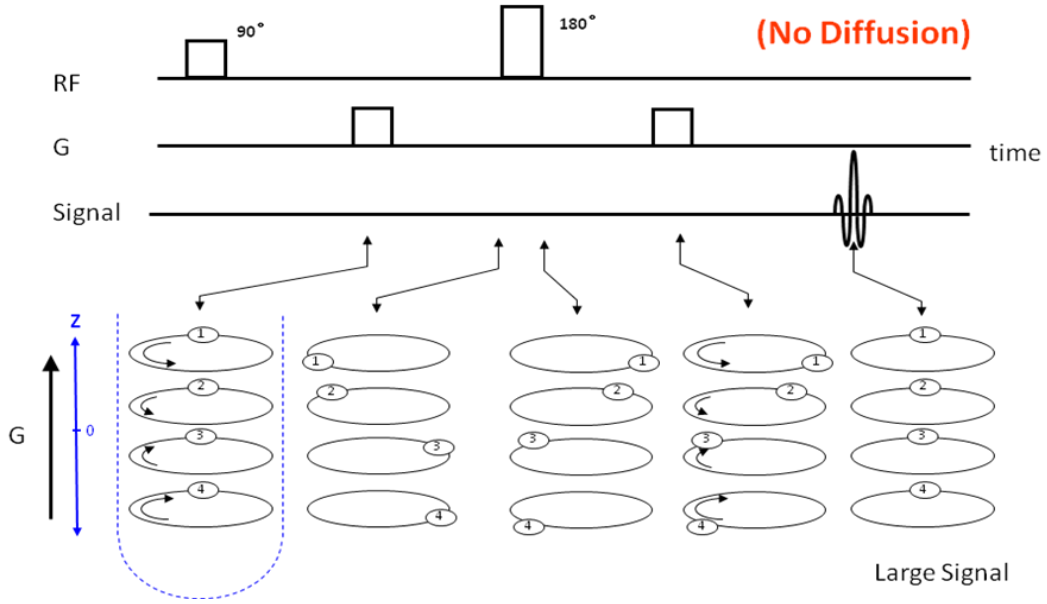

Fig. 2.9a. The race track analogy for a PGSE sequence in the absence of diffusion.

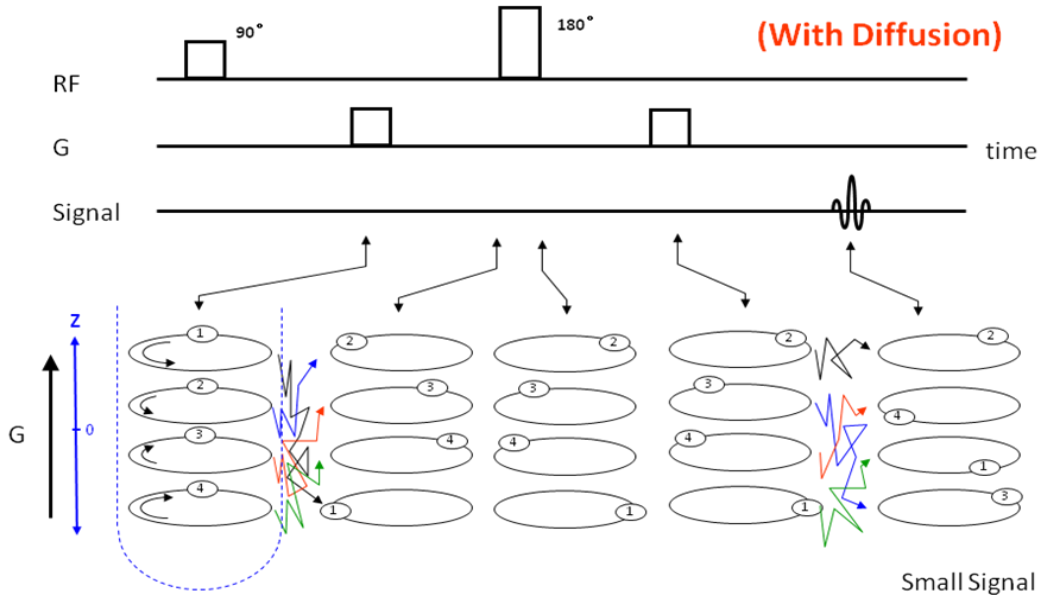

Fig. 2.9b. The race track analogy for a PGSE sequence in the presence of diffusion.

There are several variants on the PGSE pulse sequence. These variations were developed to compensate for eddy currents in the NMR system. Eddy currents are electrical currents induced in a conducting surface when exposed to a changing magnetic field. These eddy currents create their own magnetic field which distorts the desired magnetic field.

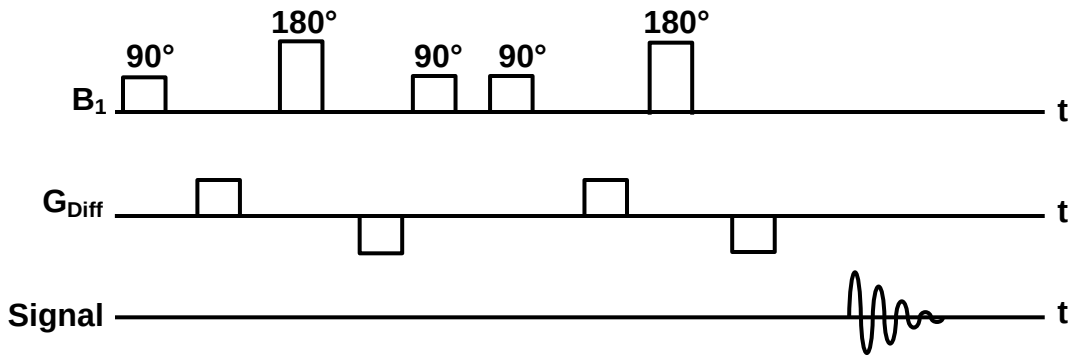

Figure 2.10 A timing diagram of the pulsed field gradient stimulated echo sequence.

Measurements of D as a function of Δ with constant δ show the effects of restricted diffusion when $\Delta \geq x_c^2 / q_i D$. Under these conditions, the measured diffusion coefficient is less than the actual diffusion coefficient for the liquid in an unrestricted environment. We have capitalized on restricted diffusion to create a phantom that will give selectable D values through the choice of Δ value and phantom orientation. An added feature of the phantom is that D is anisotropic, also allowing calibration of diffusion tensor imaging sequences. The concept is first demonstrated on small samples using the flexibility found on a high-resolution NMR spectrometer, then scaled up in size to produce a phantom for a clinical instrument.

2.4 Magnetic Resonance Imaging

The basis of all MRI is Eqn 2.6 which states that the resonance frequency is proportional to the magnetic field experienced by the nuclear spin [37, 39]. If a one-dimensional, linear, magnetic field gradient G_i is applied along direction d_i, Eqn. 2.6 becomes

$$\nu = \gamma (B_o + d_i G_i) \tag{2.20}$$

Thus the frequency becomes dependent on the location of a spin. Fourier based tomographic imaging sequences generally apply a slice selection (S) gradient followed by phase (ϕ) and frequency (f) encoding gradients to produce $N_\phi \times N_f$ pixel images of the NMR signal in a slice of thickness (Thk) through an object. The field-of-view (FOV) refers to the width of the image in distance units. All gradients and frequencies are measured relative to a point referred to as the magnet isocenter where the distances in the slice, phase, and frequency encoding directions, respectively d_S, d_ϕ, and d_f, equal zero and the resonance frequency is ν_o.

A simple 1D imaging sequence can be implemented by applying a $90^\circ B_1$ pulse followed by the application of a magnetic field gradient. (See Fig. 2.11.) This sequence is very useful for calibrating magnetic field gradients.

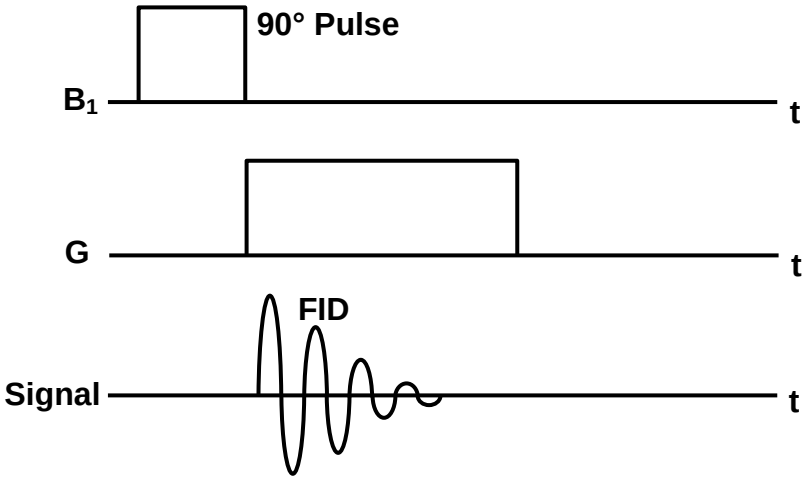

Figure 2.11 A timing diagram for a simple one-dimensional imaging sequence utilizing a 90 °-FID pulse sequence.

There are many imaging pulse sequences [41]. The echo-planar imaging sequence will be presented because it was used in this work. The echo-planar sequence is similar to a spin-echo sequence in that there are 90 °and 180 °B_1 pulses of radio frequency (RF). (See Fig. 2.12.) Positioning of a tomographic slice is achieved by the application of B_1 pulses at the same time a slice selection gradient G_s is applied. Phase and frequency encoding is achieved by the application of gradients, G_ϕ and G_f respectively, perpendicular to G_s. The signals produced by each reversal of G_f create the lines of k-space which correspond to the image. This data is Fourier transformed to create the image.

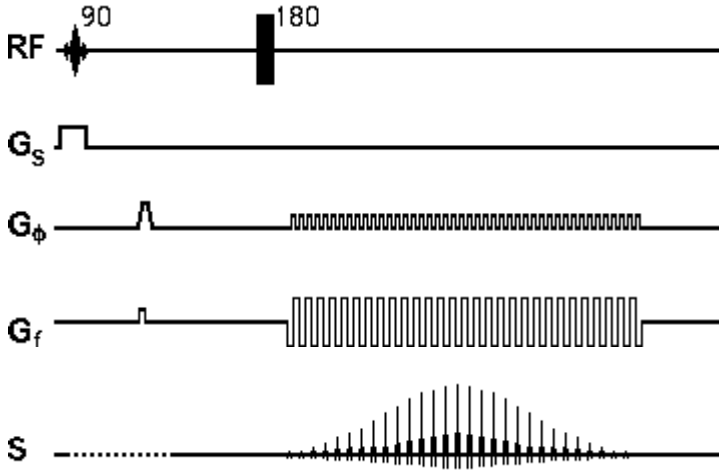

Figure 2.12. A timing diagram for a echo-planar imaging sequence. [41]

The echo-planar imaging sequence can be utilized to create diffusion images by adding the G_{Diff} pulses of Fig. 2.8. These pulses are centered about the 180 ^{o}pulse so that the last G_{Diff} pulse is completed before the succession of G_ϕ and G_f pulses. The signal in the form of an image created with G_{Diff} (S) is compared with that in the absence of G_{Diff} (S_o) using Eqn. 2.18 to obtain D. G_{Diff} can coincide with G_S, G_ϕ, or G_f, thus D can be calculated along any direction.

3.0 Experimental Methods

3.1 Sample Preparation

Several samples of poly(dimethylsiloxane) (Sigma-Aldrich, St. Louis, MO, USA), referred to as silicone oil, were used to gain experience measuring diffusion coefficients on an NMR spectrometer. These samples ranged in average molecular weight yielding viscosities of 5, 10, 20, 50, 100, 350, and 500 cSt.

Several samples of 18 MΩ·cm water in various restricted diffusion geometries were studied. NMR sample geometries included a 1 mm ID capillary tube and a 3 mm diameter hand-made bundle of 11 ± 2 μm diameter, approximately parallel, glass fiber rods held together with 0.42 cm OD shrunken heat-shrink tubing. Both samples were centered in 5 mm OD NMR tubes. The 1mm tube was filled with water, while the fiber bundle was hydrated by allowing water to be drawn up into the fibers. If fibers of diameter d are perfectly aligned and hexagonally packed, the fiber bundle creates long channels between the fibers with a maximum diffusion distance perpendicular to the long axis of the fibers of 0.732d, With this packing geometry, the water percent in the bundle is approximately 9%. Assuming a less efficient, square packing, the maximum diffusion distance perpendicular to the long axis of the fibers is d and there is 20% water in the bundle. Our packing is probably a mixture of the two packing geometries.

An optical microscope with digital camera (Eclipse E600PL, Nikon, Tokyo, Japan) and image analysis software (analySIS, Olympus Soft Imaging System GmbH, Berlin, Germany) was used to determine the diameters of the fibers in the samples.

The MRI sample geometry consisted of a 2.8 cm diameter, 9.5 cm long, hand-made bundle of 11 ± 2 μm diameter approximately parallel glass fiber rods held together with

shrink tubing. The bundle was hydrated by allowing water to be drawn up into the bundle and then it was supported in a water filled container.

The manufacturing flow chart of the 3mm diameter hand-made fiber phantom for NMR measurements is shown in Fig. 3.1. First, a bundle of parallel fibers is pulled through a piece of heat-shrinkable tubing. The tubing is shrunk to hold the fibers tightly together. This is depicted for larger fiber rods in Fig 3.1a. Second, one end of the hand-made bundle is glued together. The shrink tubing is removed once the glue is set. (See Fig. 3.1b.) The next step is to insert the bundle into an NMR tube. Once inserted, 18 MΩ·cm water is allowed to absorb into the fibers. An ultrasonic bath and vacuum are used to remove any bubble inside of the NMR tube. The diffusion is of the water between solid fiber filaments.

A scaled-up glass fiber phantom with diameter of 2.8 cm was hand-made in the similar way as that of the fiber phantom for the NMR measurements. It is used for the MRI measurements. See Fig. 3.2.

a b c

Fig. 3.1. Manufacturing flow chart for the 3mm diameter hand-made glass fiber phantom. See text for details.

Fig. 3.2. The 2.8cm diameter hand-made glass fiber phantom for MRI measurements.

3.2 NMR Spectroscopy

NMR measurements were performed on two different NMR spectrometers. Initial measurements were performed on a 300 MHz NMR spectrometer (DRX-300, Bruker Biospin, Billerica, MA, USA) with three axis gradients located at Rochester Institute of Technology (RIT). This system became inoperable after these initial measurements requiring measurements to be made on an alternative system.

A 600 MHz NMR spectrometer (UnityInova, Agilent-Varian Inc., Walnut Creek, CA, USA) with three axis gradients located at the University of Rochester was used for

all restricted diffusion measurements. Diffusion coefficients were measured at 25℃ parallel ($D_{//}$) and perpendicular ($D_{\perp}$) to the long axis of the NMR tube using a stimulated echo-pulse sequence. Each measurement of D was made from 13 b values where Δ was held constant with δ = 7 ms. The 13 values of b were achieved by varying G for the fixed Δ value to achieve b = 2, 50, 100, 150, 200, 300, 400, 500, 600, 700, 800, 900, 1000 s/mm^2. The ζ of the gradient pulses was less than with 100 μs, so ζ = 0 was used in the calculation of b. D values were measured and plotted as a function of 7 ms < Δ < 1.2s to show the effect of restricted diffusion during Δ.

3.3 Gradient Calibration

To create a diffusion standard, D must be measured accurately for the standard. This in turn requires that G and timing be known. Timing is accurately controlled by the spectrometer, but G must be measured and calibrated. There are several steps to calibrate the magnetic field gradients. The first is to determine the linearity of the gradient. The next is to determine the gradient per amp of gradient coil current. The exact procedure used differs slightly for the Z and XY gradients.

The pulse sequence of Fig. 2.11 was used to calibrate the gradients on the Bruker DRX-300 MHz NMR spectrometer at RIT. Two different sample geometries were used. For the Z gradient a small sphere of water was used. The sphere fit inside a standard 5 mm outside diameter (OD) NMR tube and could be accurately positioned along Z in the tube. (See Fig. 3.3a.) The water peak location in the spectrum was recorded and plotted for different sphere locations.

Calibrating the X and Y gradients is more challenging as there is only 4.5 mm of inside diameter (ID) to work within. The following arrangement was developed to calibrate both the X and Y gradients. A 1 mm ID capillary tube of water was secured to the inside of an NMR tube as depicted in Fig. 3.3b. The tube was connected to a goniometer located outside the NMR magnet. Finding the angles yielding the maximum and minimum resonance frequency for the water in the presence of a gradient fixed the orientation of the gradient. A series of other angles yielded a series of other locations in the gradient direction and allowed calibration of the gradient.

Determining the magnetic field per meter per amp of gradient current requires determination of the gradient at several different current values. This relationship should be linear or have a linear range.

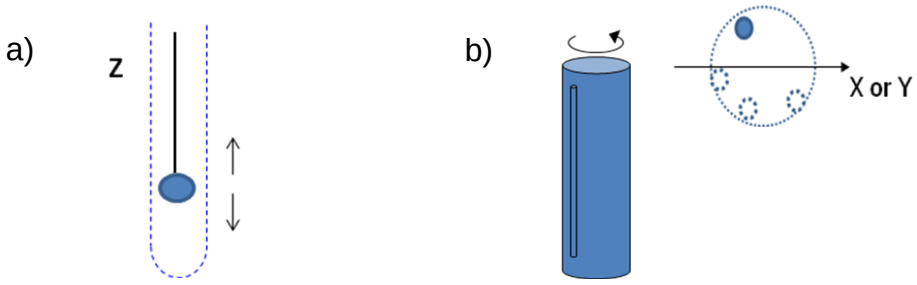

Fig. 3.1. Diagrams of the two samples used to calibrate the a) Z and b) XY gradients. The Z gradient was calibrated by moving a sphere of water along Z, while the X and Y gradients were calibrated by rotating the NMR tube with a capillary tube fixed to the inside.

3.4 MRI Measurements

All MRI measurements were performed at 20 ℃ on a 1.5 T imager (Signa Excite HDx, GE Healthcare, Waukesha, WI, USA) located at the University of Rochester. The system was operated in the research mode and utilized a diffusion-weighted, echo-planar imaging sequence, and a quadrature, bird-cage, knee RF coil. The fiber bundle was oriented so the long axis of the fibers was approximately parallel to the applied static magnetic field. An axial 5 mm thick, 15cm field-of-view imaging plane through the fibers was chosen. The stated b values (300, 500, 1000 s/mm^2) from the imager were confirmed with measured values of δ, Δ, and ζ using an oscilloscope and G taken from the control variable table. Diffusion coefficients were calculated from region-of-interest measurements from the image without the diffusion gradients yielding S and one with the diffusion gradients yielding S_o, using the imager provided b value and Eqn. (2.19).

4.0 Results and Discussion

4.1 Gradient Calibration Results

Figures 4.1 and 4.2 present the results of the calibration of the Z and X magnetic field gradients on the Bruker DRX-300 MHz NMR spectrometer at RIT. Gradient values are described in terms of their percent of the maximum value that is programmable by the spectrometer software. The Y and X gradients are assumed to be identical in geometry so only the X direction gradient was measured. Figure 4.1 shows that G_z is linear over the 2 cm long active region of the NMR probe. The three %G values are presented in Table 4.1. The change in gradient with percent gradient parameter was also linear with a value of 0.0052 T/m/%G_z. Figure 4.2 shows that G_x is also linear over 0.45 cm diameter of the NMR tube. There was more variation in G_x than G_Z, but this is attributed to the larger uncertainty in positioning the NMR tube at the desired angle. The change in G_x with percent gradient parameter was also linear with a value of 0.0028 T/m/%G_X.

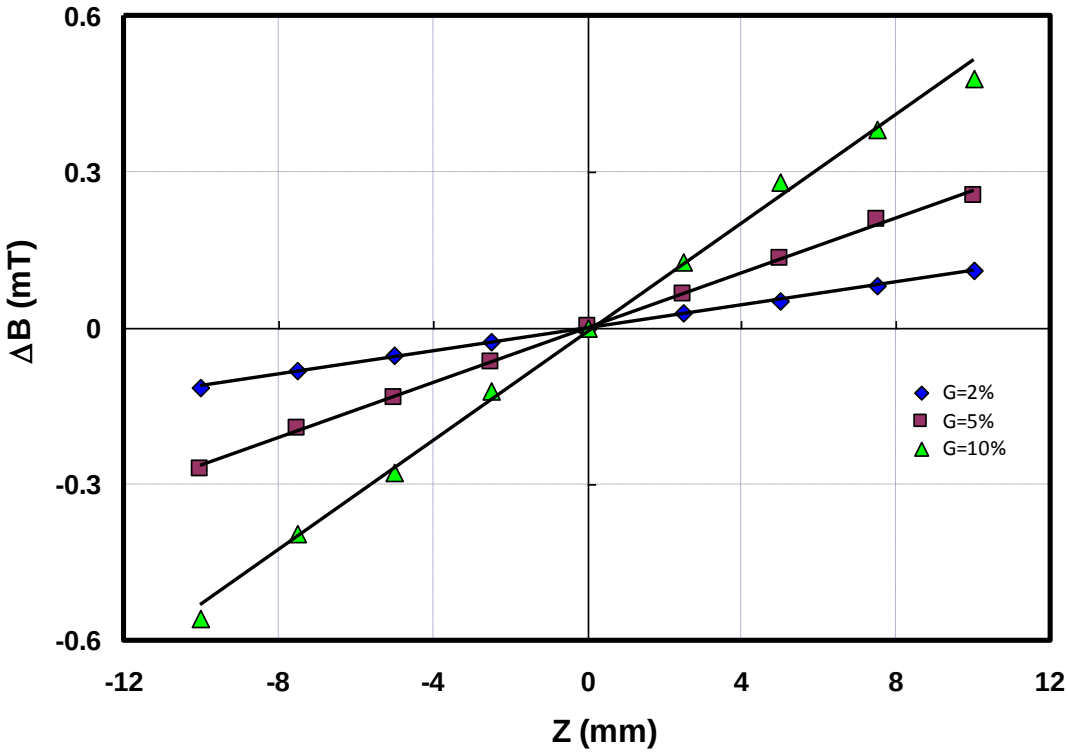

Figure 4.1. Plot of difference in magnetic field (ΔB) from its value at Z=0 as a function of location along the Z axis with 2%, 5%, and 10% of the G_Z amplitude.

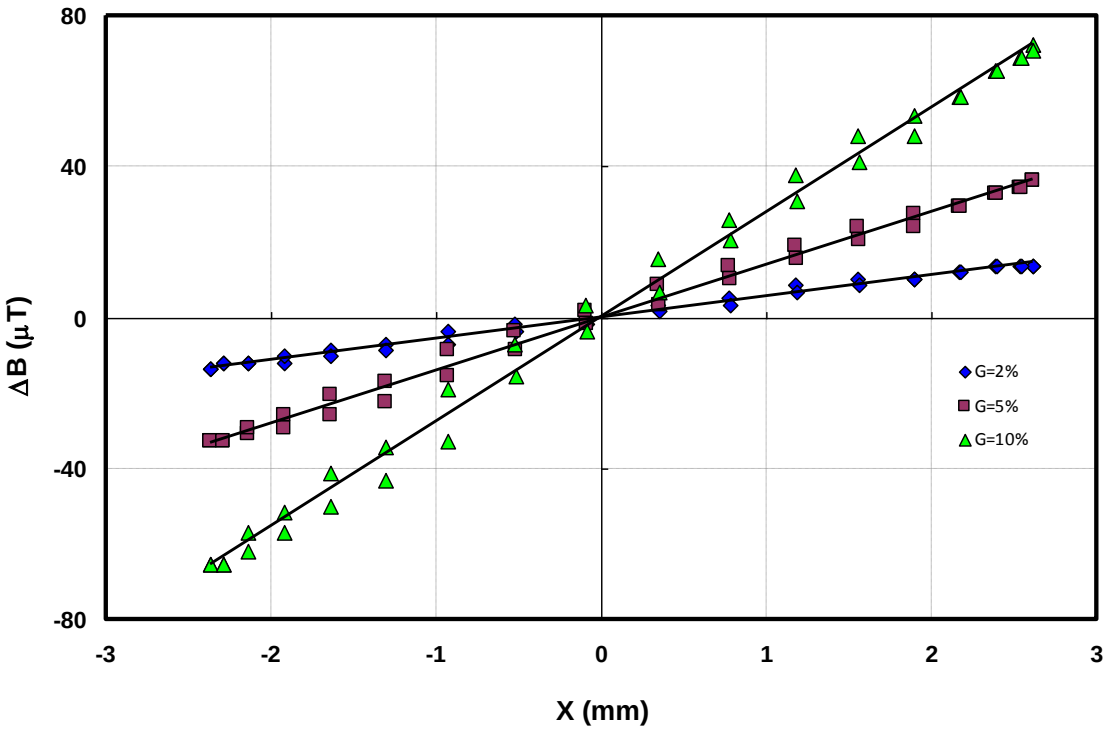

Figure 4.2. Plot of difference in magnetic field (ΔB) from its value at X=0 as a function of location along the X axis with 2%, 5%, and 10% of the G_X amplitude.

Table 4.1. G_X and G_Z for various %G settings.

%G	G (mT/m)	
	X	Z
2	5.6	11.0
5	14.0	26.5
10	27.7	52.4

4.2 Diffusion Coefficient Checks

The diffusion coefficient of water was measured at 20 ℃ using the PGSE sequence on the Bruker DRX-300 MHz NMR spectrometer at RIT. Figure 4.3 is a plot of $\ln(S/S_o)$ versus b with the solid line as the best fit to the data assuming Eqn. (2.18). The diffusion coefficient was found to be 2.32×10^{-9} m^2/s, which validates the gradient calibration.

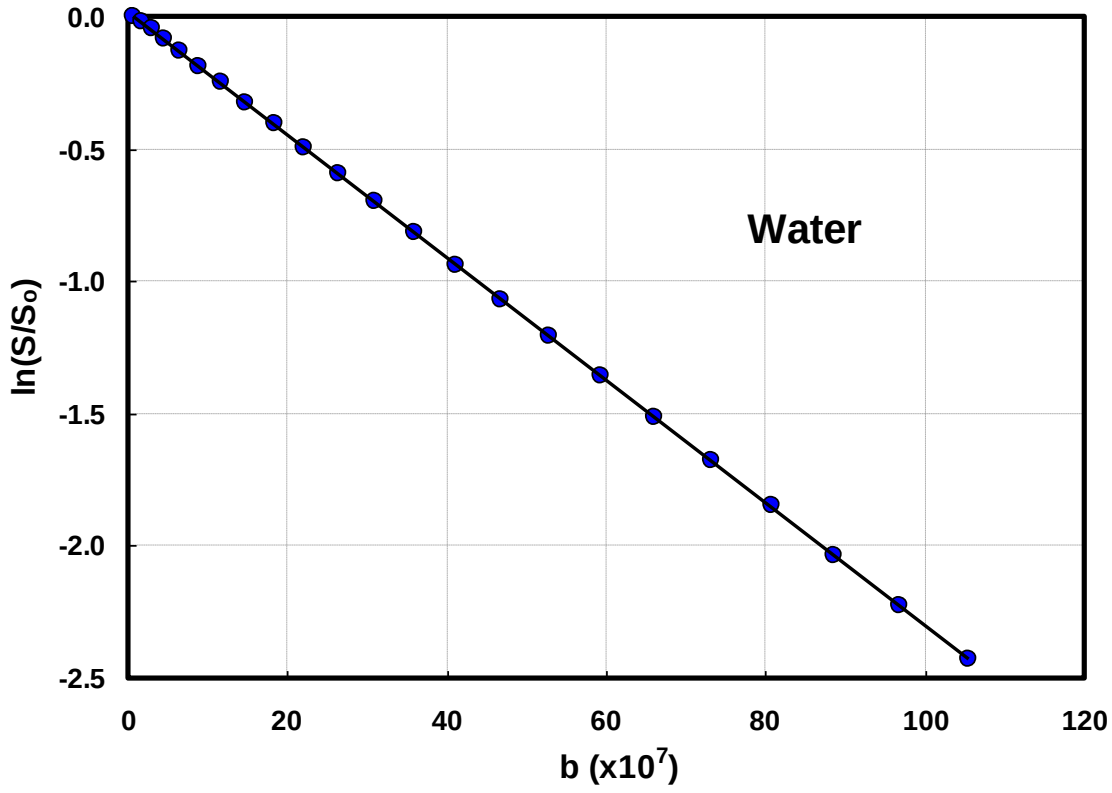

Figure 4.3. PGSE results for water at 20 ℃ indicating the change in the relative signal versus b.

The diffusion coefficient of the various molecular weight silicone oils was also measured as an additional validation on the Bruker DRX-300 MHz NMR spectrometer at RIT. These values are presented in Table 4.2 and plotted versus viscosity in Fig. 4.4. The Stokes-Einstein theory (Eqn. 2.3) predicts a linear relationship between D^{-1} and viscosity for spherical particles. The data deviated from this behavior at high molecular weights. This might be attributed to two causes. First, the molecules may behave less like spheres at higher molecular weights. The second is that the oils may contain a broader distribution of molecular weights as the average molecular weight on an oil increases.

Table 4.2. Viscosity and measured D values for Silicone Oils.

Viscosity η (cSt)	D ($\times 10^{-10}$ m^2/s)
5	1.6
10	0.73
20	0.34
50	0.11
100	0.061
350	0.025
500	0.021

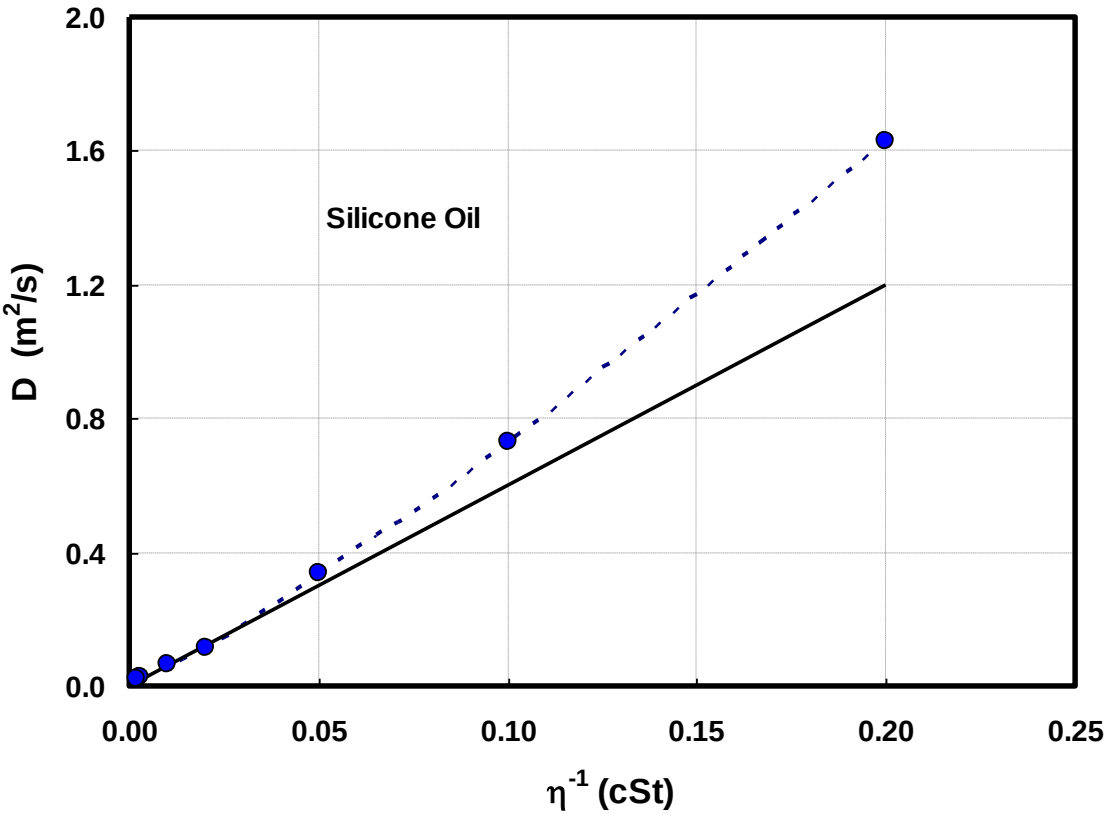

Figure 4.4. The relationship between the measured diffusion coefficient and inverse viscosity of various molecular weight silicone oils. Solid line indicates ideal Stokes-Einstein behavior and dashed line is drawn through the data to guide the eye.

4.3 Diffusion coefficients from the 600 MHz NMR

Figure 4.5 demonstrates the behavior of D as a function of $0 < \Delta < 1.2$ s for water in a 1mm ID capillary tube and the 3 mm hydrated bundle. The capillary represents unrestricted diffusion along its length ($D_{//}$) and restricted diffusion perpendicular to the length ($D_{\perp}$) of the tube. Unrestricted diffusion is demonstrated by a consistent $D_{//}$ value of 2.2×10^{-9} m^2/s over the Δ values studied. Restricted diffusion is represented by a decrease in $D_{\perp}$ from the bulk water value to 1.9×10^{-9} m^2/s with increasing Δ.

The fibers show the same general trend as the capillary tube for $D_{\perp}$. The value of $D_{\perp}$ starts at the value for bulk water and decreases to approximately 0.39×10^{-9} m^2/s. The large decrease is attributed to the smaller distance that a water molecule can diffuse perpendicular to the length of the fibers compared to the unrestricted diffusion in bulk water. The value of $D_{//}$ also shows the same trend, but only decreases to 1.4×10^{-9} m^2/s. In perfectly aligned fibers, $D_{//}$ should remain constant at a value equal to D_{Water} as Δ is increased. This tells us that the fibers in our hand-made bundle are not perfectly parallel to each other along their length. There is most likely some twisting and cross over of filaments causing the deviation from ideal behavior.

The NMR results from the glass fiber phantom are in accordance with the tendency of the Monte Carlo simulations of $D_{app}(\Delta)$ in Fieremans, et al. [29]. Their NMR measurements for a Dyneema® fiber phantom only provided values of the ADC for 4 ms $< \Delta <$ 50 ms, while we measured the apparent $D_{\perp}$ and $D_{//}$ for a larger range of 2 ms $< \Delta <$ 1.2 s. Our results for two different tendency lines of $D_{\perp}$ and $D_{//}$ with increasing Δ make it much clearer and easier to determine the fabrication performance of the fiber phantom.

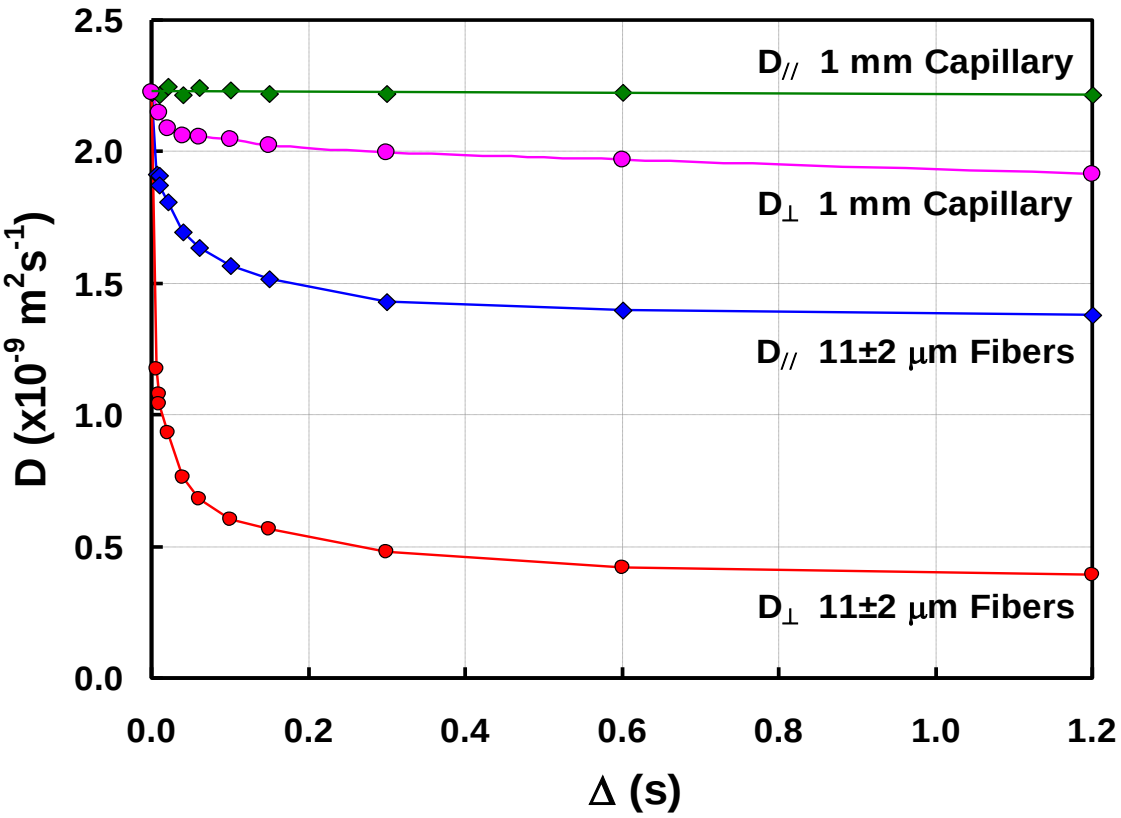

Figure 4.5. Measured D values as a function of Δ for water in a capillary tube and hydrated glass fibers using a 600 MHz high resolution NMR spectrometer at 25 ℃. Lines are drawn to guide the eye.

4.4 Diffusion Coefficients from the 1.5T MRI System

Magnetic resonance images of the scaled up, 2.8 cm diameter, glass fiber phantom are shown in Fig. 4.6. These images are from a spin echo sequence with TR/TE=500/14 ms, 256x256 matrix, and 5 mm slice thickness. The images are of good quality with surprisingly little susceptibility artifact from the large amount of glass present. A visual inspection of the image also revealed there are no air bubble artifacts in fiber bundle.

This endorsed the hydrating procedure for the bundle. Figure 4.7 shows an axial image through the phantom using an echo planar imaging diffusion sequence. This image was recorded with a 24 cm field-of-view, and TR/TE=4000/58.4 ms, and a 10 mm slice thickness.

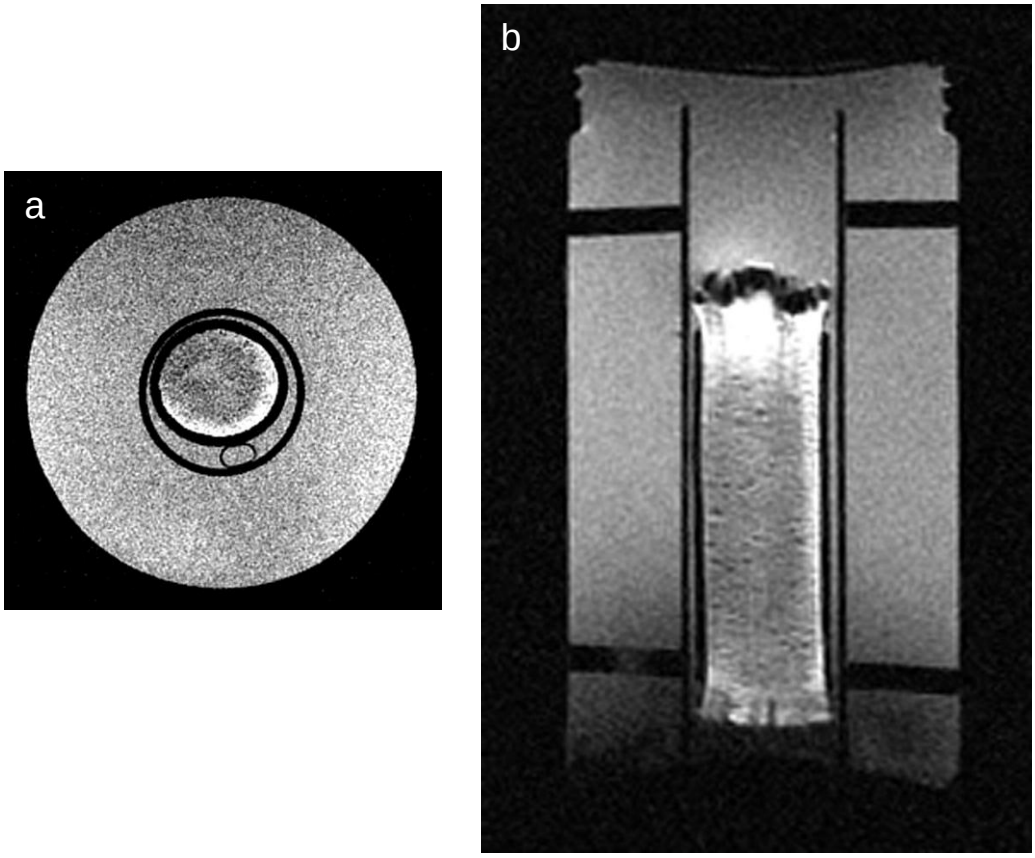

Fig. 4.6 Axial (a) and longitudinal (b) spin-echo images through the 2.8 cm fiber bundle phantom recorded at 1.5 T. Images show a lack of significant distortions despite the large amount of glass present.

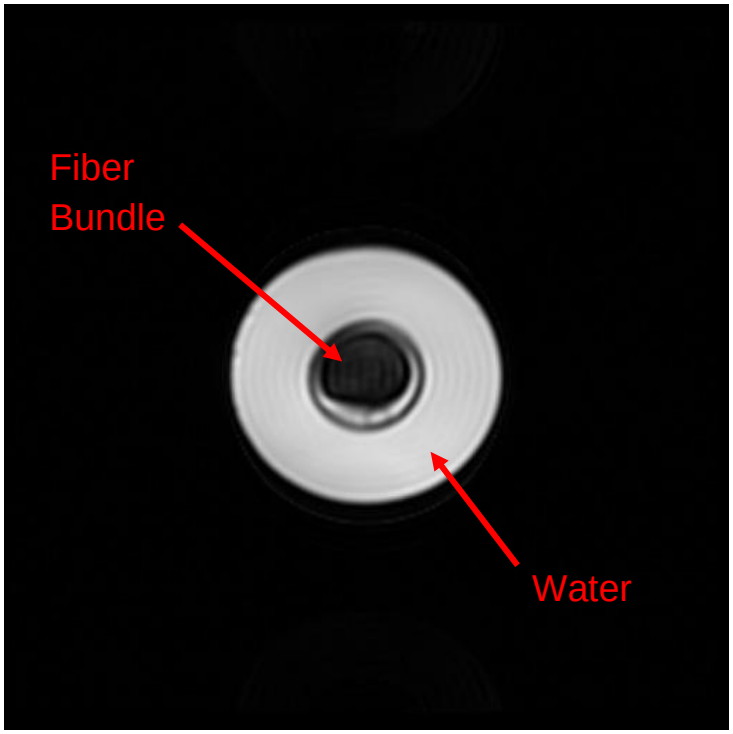

Fig. 4.7 An spin echo planar magnetic resonance image of the 2.8 cm fiber bundle phantom on a 1.5T MRI system.

Images such as that shown in Fig. 4.7 were used to calculate the magnetic resonance signal of the bulk water and the water in the fiber bundle. This signal intensity was used with Eqn. 2.18 to calculate D.

The D vs. Δ dependency for the 2.8 cm diameter bundle (Fig. 4.8.) is similar to the 3 mm bundle, but not identical. Limitations on the b values on the imager allowed us to only go to Δ = 38 ms. The value of $D_{//}$ and $D_{\perp}$ decreases from D_{Water} to respectively 1.1×10^{-9} m^2/s and 0.31×10^{-9} m^2/s in this range of Δ values. We attribute difference in D between the phantom and the NMR tube fiber bundles to the ~5 ℃ temperature difference for the measurements, our limited ability to achieve identical packing of the two hand-

made fiber bundles, and that ROIs where used in the phantom measures while whole sample measures were used in the NMR tube bundles.

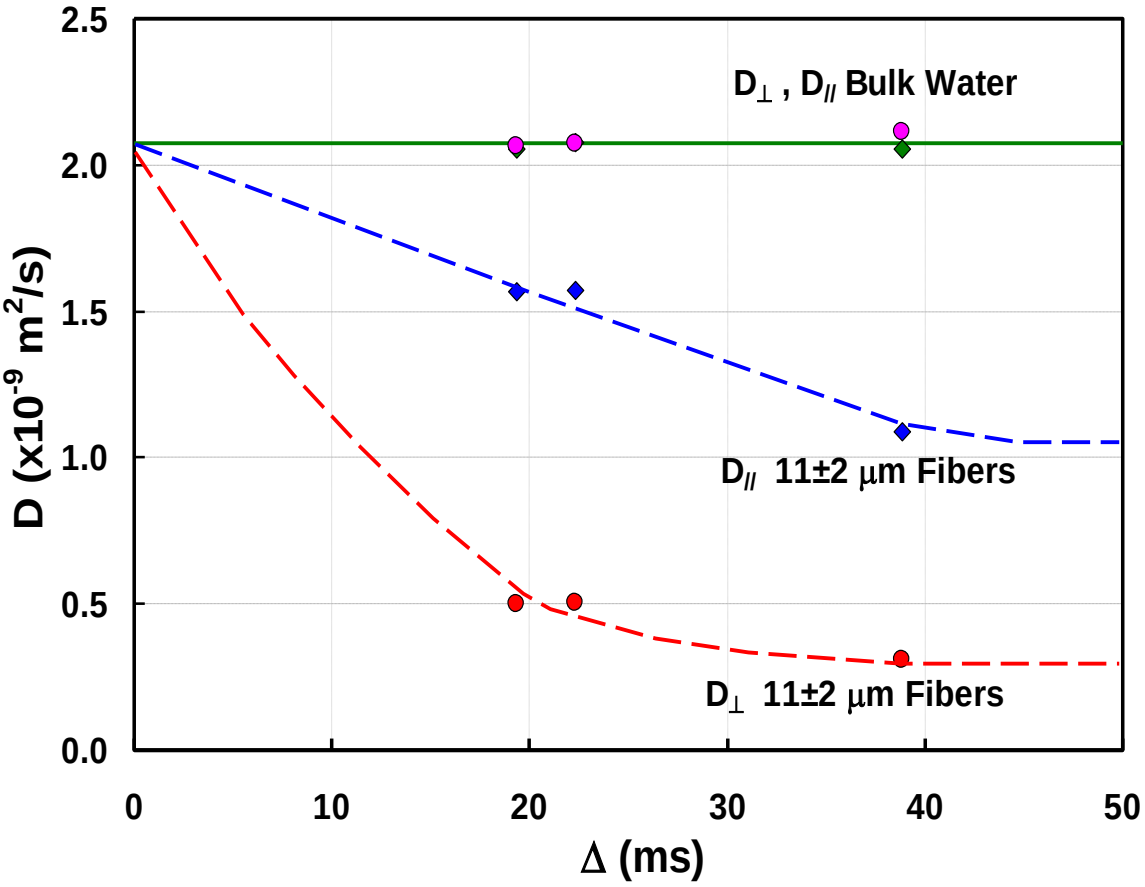

Figure 4.8 Measured D values as a function of Δ for bulk water and hydrated glass fibers using a 1.5T clinical MRI system at 20 ℃. Lines are drawn to guide the eye.

The result demonstrated that a series of diffusion coefficient values, in a range of D_{water} and approximately 0.5×10^{-9} m^2/s, can be obtained with selected data acquisition parameter Δ, and a fully hydrated, tightly packed fiber bundle. The greatest challenge in constructing the fiber bundle is keeping the fibers perfectly parallel to each other. Perhaps machine packing will help achieve this.

5.0 Conclusions

A simple, mathematical-based, multi-point method was used to calibrate the Z and X magnetic field gradients on the Bruker DRX-300 MHz NMR spectrometer at RIT. Results of both the Z and X direction gave, as expected, very linear gradients across the space of a sample and very linear relationship between the prescribed and measured gradient strength.

When this gradient calibration was used to measure the self diffusion coefficient of pure water on the Bruker spectrometer, the measured value matched the literature value. The similarity of these two diffusion coefficient values also validated the calibration of the gradients.

The diffusion coefficient of silicone oil as a function of viscosity deviated slightly from the ideal Stokes-Einstein linear relationship. This deviation is thought to be attributed to the presence of a broader distribution of molecular weight values and a deviation from spherical particles as the molecular weight increases.

The NMR results from the 3 mm diameter fiber bundle phantom show the behavior of the restricted diffusion over a range two orders of magnitude in Δ. This range is greater than that reported previously in the literature. These results also demonstrate the potential of using restricted water diffusion in fiber bundles to achieve diffusion standards with a diffusion coefficient between D_{Water} and 0.5×10^{-9} m^2/s without utilizing flammable hydrocarbons. The use of such phantoms as diffusion standards will reduce shipping costs because of the absence of flammable hydrocarbons.

According to our experiments, the measured diffusion coefficient in the bundles of glass fiber is dependent on the parallel alignment of the fiber bundles. Machine made

bundles should provide high parallel alignment of the fibers as well as highly reproducible diffusion properties within such glass fiber phantoms, despite some variability of the measurements of the diffusion coefficient of water.

Future work on this topic might involve a study of D vs. Δ for more perfectly aligned hydrated fibers in a bundle.

References

1. Bach, D. S.; Armstrong, W. F.; Donovan, C. L.; Muller, D. W., Quantitative Doppler Tissue Imaging for Assessment of Regional Myocardial Velocities during Transient Ischemia and Reperfusion. *Am Heart J* **1996,** *132* (4), 721-725.
2. Fox, R. J.; Cronin, T.; Lin, J.; Wang, X.; Sakaie, K.; Ontaneda, D.; Mahmoud, S. Y.; Lowe, M. J.; Phillips, M. D., Measuring Myelin Repair and Axonal Loss with Diffusion Tensor Imaging. *AJNR Am J Neuroradiol* **2011,** *32* (1), 85-91.
3. Heemskerk, A. M.; Drost, M. R.; van Bochove, G. S.; van Oosterhout, M. F.; Nicolay, K.; Strijkers, G. J., DTI-based Assessment of Ischemia-reperfusion in Mouse Skeletal Muscle. *Magn Reson Med* **2006,** *56* (2), 272-281.
4. Song, S. K.; Sun, S. W.; Ju, W. K.; Lin, S. J.; Cross, A. H.; Neufeld, A. H., Diffusion Tensor Imaging Detects and Differentiates Axon and Myelin Degeneration in Mouse Optic Nerve after Retinal Ischemia. *Neuroimage* **2003,** *20* (3), 1714-1722.
5. Okumura, A.; Fukatsu, H.; Kato, K.; Ikuta, T.; Watanabe, K., Diffusion Tensor Imaging in Frontal Lobe Epilepsy. *Pediatr Neurol* **2004,** *31* (3), 203-206.
6. Rugg-Gunn, F. J.; Eriksson, S. H.; Symms, M. R.; Barker, G. J.; Thom, M.; Harkness, W.; Duncan, J. S., Diffusion Tensor Imaging in Refractory Epilepsy. *Lancet* **2002,** *359* (9319), 1748-1751.
7. Winston, G. P.; Yogarajah, M.; Symms, M. R.; McEvoy, A. W.; Micallef, C.; Duncan, J. S., Diffusion Tensor Imaging Tractography to Visualize the Relationship of the Optic Radiation to Epileptogenic Lesions Prior to Neurosurgery. *Epilepsia* **2011**.

8. Inoue, T.; Ogasawara, K.; Beppu, T.; Ogawa, A.; Kabasawa, H., Diffusion Tensor Imaging for Preoperative Evaluation of Tumor Grade in Gliomas. *Clin Neurol Neurosurg* **2005,** *107* (3), 174-180.

9. Li, X.; Yu, R. T.; Xu, K.; Li, F. C.; Fan, Y. C.; Gao, W. C.; Guo, K. Q.; Pan, X.; Yang, C., Application of Diffusion Tensor Imaging in Preoperation and Postoperation Patients of Glioma with 3.0 Tesla MRI. *Zhonghua Yi Xue Za Zhi* **2009,** *89* (19), 1300-1304.

10. Moffat, B. A.; Hall, D. E.; Stojanovska, J.; McConville, P. J.; Moody, J. B.; Chenevert, T. L.; Rehemtulla, A.; Ross, B. D., Diffusion Imaging for Evaluation of Tumor Therapies in Preclinical Animal Models. *MAGMA* **2004,** *17* (3-6), 249-259.

11. Lee, J. S.; Han, M. K.; Kim, S. H.; Kwon, O. K.; Kim, J. H., Fiber Tracking by Diffusion Tensor Imaging in Corticospinal Tract Stroke: Topographical Correlation with Clinical Symptoms. *Neuroimage* **2005,** *26* (3), 771-776.

12. Parmar, H.; Golay, X.; Lee, K. E.; Hui, F.; Sitoh, Y. Y., Early Experiences with Diffusion Tensor Imaging and Magnetic Resonance Tractography in Stroke Patients. *Singapore Med J* **2006,** *47* (3), 198-203.

13. Werring, D. J.; Toosy, A. T.; Clark, C. A.; Parker, G. J.; Barker, G. J.; Miller, D. H.; Thompson, A. J., Diffusion Tensor Imaging Can Detect and Quantify Corticospinal Tract Degeneration After Stroke. *J Neurol Neurosurg Psychiatry* **2000,** *69* (2), 269-272.

14. Delakis, I.; Moore, E. M.; Leach, M. O.; De Wilde, J. P., Developing A Quality Control Protocol for Diffusion Imaging on A Clinical MRI System. *Phys Med Biol* **2004,** *49* (8), 1409-1422.

15. Laubach, H. J.; Jakob, P. M.; Loevblad, K. O.; Baird, A. E.; Bovo, M. P.; Edelman, R. R.; Warach, S., A Phantom for Diffusion-weighted Imaging of Acute Stroke. *J Magn Reson Imaging* **1998,** *8* (6), 1349-1354.

16. Matsuya, R.; Kuroda, M.; Matsumoto, Y.; Kato, H.; Matsuzaki, H.; Asaumi, J.; Murakami, J.; Katashima, K.; Ashida, M.; Sasaki, T.; Sei, T.; Himei, K.; Katsui, K.; Katayama, N.; Takemoto, M.; Kanazawa, S.; Mimura, S.; Oono, S.; Kitayama, T.; Tahara, S.; Inamura, K., A New Phantom Using Polyethylene Glycol As An Apparent Diffusion Coefficient Standard for MR Imaging. *Int J Oncol* **2009,** *35* (4), 893-900.

17. Tofts, P. S.; Lloyd, D.; Clark, C. A.; Barker, G. J.; Parker, G. J.; McConville, P.; Baldock, C.; Pope, J. M., Test Liquids for Quantitative MRI Measurements of Self-diffusion Coefficient in Vivo. *Magn Reson Med* **2000,** *43* (3), 368-374.

18. Boujraf, S.; Luypaert, R.; Eisendrath, H.; Osteaux, M., Echo Planar Magnetic Resonance Imaging of Anisotropic Diffusion in Asparagus Stems. *MAGMA* **2001,** *13* (2), 82-90.

19. Hills, B.; Knovel (Firm), *Magnetic Resonance Imaging in Food Science*; Wiley: New York, 1998; p160, 342 p.

20. Lätt, J.; Nilsson, M.; Rydhög, A.; Wirestam, R.; Ståhlberg, F.; Brockstedt, S., Effects of Restricted Diffusion in A Biological Phantom: A q-space Diffusion MRI Study of Asparagus Stems at A 3T Clinical Scanner. *MAGMA* **2007,** *20* (4), 213-222.

21. Madi, S.; Hasan, K. M.; Narayana, P. A., Diffusion Tensor Imaging of in Vivo And Excised Rat Spinal Cord at 7 T with An Icosahedral Encoding Scheme. *Magn Reson Med* **2005,** *53* (1), 118-125.

22. Trudeau, J. D.; Dixon, W. T.; Hawkins, J., The Effect of Inhomogeneous Sample Susceptibility on Measured Diffusion Anisotropy Using NMR Imaging. *J Magn Reson B* **1995,** *108* (1), 22-30.

23. Lin, C. P.; Wedeen, V. J.; Chen, J. H.; Yao, C.; Tseng, W. Y., Validation of Diffusion Spectrum Magnetic Resonance Imaging with Manganese-enhanced Rat Optic Tracts and Ex Vivo Phantoms. *Neuroimage* **2003,** *19* (3), 482-495.

24. von dem Hagen, E. A.; Henkelman, R. M., Orientational Diffusion Reflects Fiber Structure within A Voxel. *Magn Reson Med* **2002,** *48* (3), 454-459.

25. Yanasak, N.; Allison, J., Use of Capillaries in The Construction of An MRI Phantom for The Assessment of Diffusion Tensor Imaging: Demonstration of Performance. *Magn Reson Imaging* **2006,** *24* (10), 1349-1361.

26. Fieremans, E.; Delputte, S.; Deblaere, K.; De Deene, Y.; Truyens, B.; D'Asseler, Y.; Achten, E.; Lemahieu, I.; Van de Walle, R., A Flexible Hardware Phantom for Validation of Diffusion Imaging Sequences, *Proceeding of the ISMRM 13th scientific meeting*, Miami, USA, 2005, p. 1301.

27. Perrin, M.; Poupon, C.; Rieul, B.; Leroux, P.; Constantinesco, A.; Mangin, J. F.; Lebihan, D., Validation of Q-ball Imaging with A Diffusion Fibre-crossing Phantom on A Clinical Scanner. *Philos Trans R Soc Lond B Biol Sci* **2005,** *360* (1457), 881-891.

28. Lorenz, R.; Bellemann, M. E.; Hennig, J.; Il'yasov, K. A., Anisotropic Phantoms for Quantitative Diffusion Tensor Imaging and Fiber-tracking Validation. *Applied Magnetic Resonance* **2008,** *33* (4), 419-429.

29. Fieremans, E.; De Deene, Y.; Delputte, S.; Ozdemir, M. S.; D'Asseler, Y.; Vlassenbroeck, J.; Deblaere, K.; Achten, E.; Lemahieu, I., Simulation And Experimental Verification of The Diffusion in An Anisotropic Fiber Phantom. *J Magn Reson* **2008,** *190* (2), 189-199.

30. http://www.dyneema.com/en_US/public/dyneema/page/about/Material.htm.

31. Mulkern, R.V.; Zengingonul, H.P.; Robertson, R.L.; Bogner, P.; Zou, K.H.; Gudbjatsson, H.; Guttmann, C.R.; Holtzman, D.; Kyriakos, W.; Jolesz, F.A.,;Maier, S.E., Multi-component Apparent Diffusion Coefficients in Human Brain: Relationship to Spin-Lattice Relaxation. *Magn. Reson. Med*. **2000**, *44*, 292-300.

32. Poupon, C.; Rieul, B; Kezele, I; Perrin, M; Poupon, F; Mangin, J.F., New Diffusion Phantoms Dedicated to The Study and Validation of High-angular-resolution Diffusion Imaging (HARDI) Models. *Magn Reson Med* **2008**, *60*, 1276–1283.

33. Komlosh, M.E.; Horkay, F.; Freidlin, R.Z.; Nevo, U.; Assaf, Y.; Basser, P.J., Detection of Microscopic Anisotropy in Gray Matter and In A Novel Tissue Phantom Using Double Pulsed Gradient Spin Echo MR. *J Magn Reson* **2007**, *189*, 38-45.

34. Sadleir, R.J.; Neralwala, F.; Te, T.; Tucker, A., A Controllably Anisotropic Conductivity or Diffusion Phantom Constructed from Isotropic Layers. *Annal Biomed Eng* **2008**, *37*, 2522-2531.

35. Ogrezeanu, G.; Hartlep, A., Fiber Tracking Phantom. US Patent 7521931, April 21, **2009**.

36. Smith, W. F.; Hashemi, J., *Foundations of Materials Science and Engineering*. 3rd ed.; McGraw-Hill: Boston [Mass.], 2004; 908 p.

37. Price, W.S., Pulsed-field Gradient Nuclear Magnetic Resonance As A Tool for Studying Translational Diffusion: Part 1. Basic theory. *Concepts Magn Reson* **1997**, *9*, 299-336.

38. Stejskal, E.O.; Tanner, J.E., Spin Diffusion Measurements: Spin Echoes in The Presence of A Time-dependent Field Gradient. *J. Chem. Phys.* **1965**, *42*, 288-292.

39. Hornak, J. P., *The Basics of MRI*. Interactive Learning Software, Henrietta, NY. http://www.cis.rit.edu/htbooks/mri/.

40. Akitt, J. W.; Mann, B. E., *NMR and chemistry : An Introduction to Modern NMR Spectroscopy*. 4th ed.; S. Thornes: Cheltenham, U.K., 2000; 400 p.

41. Bernstein, M. A.; King, K. F.; Zhou, X. J., *Handbook of MRI Pulse Sequences*. Academic Press: Amsterdam ; Boston, 2004; p xxii,1017 p.